JOURNAL OF PROPULSION AND POWER
Vol. 24, No. 6, November–December 2008

Survey of Aerodynamic Drag Reduction at High Speed by Energy Deposition

D. Knight*
Rutgers University, Piscataway, New Jersey 08854-8058

DOI: 10.2514/1.24595

A selected survey of aerodynamic drag reduction at high speed is presented. The dimensionless governing parameters are described for energy deposition in an ideal gas. The types of energy deposition are divided into two categories. First, energy deposition in a uniform supersonic flow is discussed. Second, energy deposition upstream of a simple aerodynamic body is examined. Both steady and unsteady (pulsed) energy deposition are examined for both categories, as well as the conditions for the formation of shock waves and recirculation regions. The capability of energy deposition to reduce drag is demonstrated experimentally. Areas for future research are briefly discussed.

Nomenclature

A	=	cross-sectional area
C_D	=	drag coefficient
c_p	=	specific heat at constant pressure
D	=	diameter of body
d	=	diameter of filament
$\mathcal{G}, \tilde{\mathcal{G}}$	=	spatial distribution functions for energy deposition
I	=	impulse
L	=	streamwise length
ℓ	=	characteristic length
M	=	freestream Mach number
$\dot{m}$	=	mass flow rate
P	=	power
p	=	pressure
Q	=	energy added per unit volume per time
Q_o	=	magnitude of energy deposition (energy per unit volume per time)
Q_T	=	energy deposited in V in time interval τ_e
q	=	energy added per unit mass per time
q_o	=	magnitude of energy deposition (energy per unit mass per time)
q_T	=	energy per mass deposited in V in time interval τ_e
R	=	gas constant for air
T	=	temperature
$\mathcal{T}$	=	temporal distribution function for energy deposition
U	=	freestream velocity
V	=	volume
$\boldsymbol{v}$	=	velocity
α	=	ρ_f/ρ_∞
γ	=	ratio of specific heats
ΔE_f	=	energy added
$\delta_e, \delta_i, \delta_L$	=	dimensionless time scales
$\varepsilon, \varepsilon'$	=	energy deposition parameters
η	=	efficiency of energy deposition
ρ	=	density
ϖ	=	ratio of energy added to energy required to choke the flow
σ	=	dimensionless time parameter
τ_e	=	duration of energy pulse

Subscripts

f	=	filament
∞	=	freestream

I. Overview

IN RECENT years, there has been intense activity in developing a fundamental understanding and practical applications of flow control at high speed using energy deposition. This interest is reflected in numerous conferences and workshops, including the Weakly Ionized Gas Workshops [1–8], the St. Petersburg Workshops [9–12], and the Institute for High Temperatures Workshops [13–19]. The scope of this research is broad. It encompasses a wide variety of energy deposition techniques (e.g., plasma arcs, laser pulse, microwave, electron beam, glow discharge, etc.) and a wide range of applications (e.g., drag reduction, lift and moment enhancement, improved combustion and mixing, modification of shock structure, etc.).

The objective of this paper is to provide a selective survey of research on aerodynamic drag reduction at high speed using energy deposition. The research is reviewed principally from the viewpoint of ideal gas dynamics to elucidate the thermal effects of energy deposition on supersonic flow. In general, nonideal gas effects are not considered (except insofar as they naturally occur in the experiments cited herein) and are the topic of a future survey.

The remainder of this paper is divided into three sections. Section II summarizes the governing equations and relevant dimensionless parameters for energy deposition in an ideal gas. Section III focuses on steady and unsteady energy deposition in uniform supersonic flow in the absence of an aerodynamic body. The understanding of this simple class of flows is essential for the interpretation of energy deposition in the presence of an aerodynamic shape. Section IV considers steady and unsteady energy deposition in the presence of an aerodynamic body from the viewpoint of drag reduction.

This survey is necessarily selective and restrictive due to the substantial literature on this topic. Additional reviews can be found in Zheltovodov [20], Fomin et al. [21], and Bletzinger et al. [22]. Related research in magnetoaerodynamics is reviewed, for example, in Shang [23].

II. Governing Equations

The physics of energy deposition in high speed flows is multidisciplinary. In this paper, we consider energy deposition from the viewpoint of a perfect gas. Admittedly, this is an approximation of the actual physics because nonideal gas effects may be relevant due to the nature of the energy deposition (e.g., the formation of a plasma due to a laser or microwave pulse). Nevertheless, many of the salient features of flow control by energy deposition are elucidated

Received 12 April 2006; revision received 7 July 2008; accepted for publication 7 July 2008.

*Professor, Department of Mechanical and Aerospace Engineering, 98 Brett Road. Associate Fellow AIAA.

from this somewhat restricted viewpoint, which serves as a basis for understanding.

The governing equations for energy deposition in an inviscid perfect gas are

$$\frac{\partial \rho}{\partial t} + \nabla \cdot \rho \boldsymbol{v} = 0 \tag{1}$$

$$\frac{\partial \boldsymbol{v}}{\partial t} + \boldsymbol{v} \cdot \nabla \boldsymbol{v} = -\frac{1}{\rho} \nabla p \tag{2}$$

$$\frac{\partial T}{\partial t} + \boldsymbol{v} \cdot \nabla T = -(\gamma - 1) T \nabla \cdot \boldsymbol{v} + \frac{Q}{\rho c_v} \tag{3}$$

where ρ is the density, $\boldsymbol{v}$ is the velocity, p is the static pressure, T is the static temperature, and Q is the energy added per unit volume per time.

We define the dimensionless parameters relevant to three-dimensional energy deposition in a perfect, inviscid gas under certain simplifying assumptions. The energy deposition is assumed to be given by

$$Q = Q_o \mathcal{G}(x/\ell, y/\ell, z/\ell) \mathcal{T}(t/\tau_e) \tag{4}$$

where Q_o is the characteristic dimensional magnitude of the energy deposition (units of energy per unit volume per time) and $\mathcal{G}$ defines the dimensionless spatial distribution of energy deposition in an effective volume V with

$$\frac{1}{V} \int_V \mathcal{G} \, \mathrm{d}V = 1 \tag{5}$$

Without loss of generality, it may be assumed that

$$\mathcal{G}(0, 0, 0) = 1 \tag{6}$$

which, together with Eqs. (4) and (5), serves to define the characteristic volume V of the energy deposition. An example is

$$\mathcal{G} = e^{-(r/r_o)^2} \tag{7}$$

where $r^2 = (x - x_o)^2 + (y - y_o)^2 + (z - z_o)^2$ and (x_o, y_o, z_o) is the center of the energy deposition region and $\ell = r_o$ is the characteristic length scale. This satisfies $\mathcal{G}(0, 0, 0) = 1$ and, from Eq. (5), $V = \pi^{3/2} r_o^3$. The dimensionless temporal dependence $\mathcal{T}$ may be assumed normalized so that

$$\frac{1}{\tau_e} \int_t^{t+\tau_e} \mathcal{T} \, \mathrm{d}t = 1 \tag{8}$$

where τ_e is the duration of the energy pulse. For steady energy deposition, $\mathcal{T} = 1$. The total energy deposited within the volume V in the time interval τ_e is therefore

$$Q_T = \int_t^{t+\tau_e} \int_V Q \, \mathrm{d}V \, \mathrm{d}t \tag{9}$$

The total energy per unit effective volume deposited in time τ_e is therefore

$$Q_o = (Q_T / V \tau_e) \tag{10}$$

For steady energy deposition,

$$Q_o = \frac{1}{V} \int_V Q \, \mathrm{d}V \tag{11}$$

The effect of energy deposition on the flowfield, either alone or in the presence of a body, depends upon several dimensionless factors. The first is a dimensionless energy deposition parameter defined as

$$\varepsilon = \frac{Q_T}{\rho_\infty c_p T_\infty V + \rho_\infty c_p T_\infty U_\infty A \tau_e} \tag{12}$$

The numerator is the energy deposition in V at time τ_e. The denominator is the sum of two terms. The first term is the static enthalpy in region V at the beginning of the energy pulse. The second term is the static enthalpy flux through the cross-sectional area A during the characteristic time scale of the energy deposition τ_e. Thus,

$$\varepsilon = \frac{(\gamma - 1)}{\gamma} \frac{Q_T}{p_\infty V} \frac{1}{(1 + U_\infty \tau_e / \ell)} \tag{13}$$

with

$$A = V / \ell \tag{14}$$

For steady energy deposition (i.e., $U_\infty \tau_e / \ell \to \infty$), Eq. (12) reduces to

$$\varepsilon = (\gamma - 1) \frac{M_\infty^2 Q_o \ell}{\rho_\infty U_\infty^3} \tag{15}$$

using Eq. (10). For periodic energy deposition, the first term in the denominator in Eq. (12) is not relevant, and ε is given by Eq. (15) where Q_o represents the energy deposition per unit volume and time during the energy pulse [see Eq. (10)].

Another definition can be formed assuming the energy deposition is expressed as

$$Q = \rho q \tag{16}$$

where q is the energy added per unit mass per time. An expression for q similar to Eq. (4) is

$$q = q_o \tilde{\mathcal{G}}(x/\ell, y/\ell, z/\ell) \tilde{\mathcal{T}}(t/\tau_e) \tag{17}$$

where q_o is the characteristic dimensional magnitude of the energy deposition (units of energy per unit mass per time) and $\tilde{\mathcal{G}}(x/\ell, y/\ell, z/\ell)$ defines the dimensionless spatial distribution of energy deposition in a finite volume V with

$$\frac{1}{V} \int_V \tilde{\mathcal{G}} \, \mathrm{d}V = 1 \tag{18}$$

and $\tilde{\mathcal{G}}(0, 0, 0) = 1$. Also,

$$\frac{1}{\tau_e} \int_t^{t+\tau_e} \tilde{\mathcal{T}} \, \mathrm{d}t = 1 \tag{19}$$

Then, by analogy,

$$q_T = \int_t^{t+\tau_e} \int_V q \, \mathrm{d}V \, \mathrm{d}t \tag{20}$$

For steady energy deposition,

$$q_o = \frac{1}{V} \int_V q \, \mathrm{d}V \tag{21}$$

The corresponding dimensionless energy deposition parameter is

$$\varepsilon' = \frac{q_T}{c_p T_\infty V + c_p T_\infty U_\infty A \tau_e} \tag{22}$$

where A is defined by Eq. (14). This yields

$$\varepsilon' = \frac{(\gamma - 1)}{\gamma} \frac{\rho_\infty q_T}{p_\infty V} \frac{1}{(1 + U_\infty \tau_e / \ell)} \tag{23}$$

For steady flow,

$$\varepsilon' = (\gamma - 1) \frac{M_\infty^2 q_o \ell}{U_\infty^3} \tag{24}$$

Table 1 Parameters

Parameter	Relation
ε, ε'	Energy deposition
δ_e	Pulse duration
δ_i	Pulse interval
δ_L	Pulse interval
M_∞	Mach number
γ	Ratio of specific heats
$\mathcal{G}$	Energy spatial distribution function
$\mathcal{T}$	Energy temporal distribution function

The second through fourth parameters are dimensionless ratios of time scales:

$$\delta_e = \tau_e/(\ell/U_\infty) \tag{25}$$

$$\delta_i = \tau_i/(\ell/U_\infty) \tag{26}$$

$$\delta_L = \tau_i/(L/U_\infty) \tag{27}$$

where τ_e is the duration of the energy pulse, τ_i is the time interval between energy pulses, and L is a characteristic distance between the energy deposition region and the body. The first and second parameters relate the duration and time interval of the energy pulse to the timescale associated with the flow transiting the streamwise dimension ℓ of the energy deposition region. For example, $\delta_e \ll 1$ implies that the energy deposition is virtually instantaneous, that is, the fluid has moved a negligible distance during the time of the energy deposition. This is typical of a pulsed laser energy deposition. Additionally, $\delta_i \gg 1$ implies that the interval between energy pulses (assuming $\tau_e \ll \tau_i$) is large compared with the time required for the fluid to move through the energy deposition region. The fourth parameter relates the time interval of the energy pulse to the time scale associated with the flow transiting the streamwise distance L between the energy deposition region and the body. For example, if $\delta_L \ll 1$, then the modification to the flowfield in the vicinity of the body is quasi stationary.

The remaining parameters are the Mach number M_∞ and ratio of specific heats γ. In addition, the flowfield depends upon the body shape itself and the location of the energy deposition relative to the body. The parameters are summarized in Table 1.

III. Energy Deposition in Uniform Supersonic Flow

In this section, we consider steady and unsteady energy deposition in uniform supersonic flow in the absence of any aerodynamic body.

A. Steady Energy Deposition

Linear, weakly nonlinear, and strongly nonlinear solutions of Eqs. (1–3) have been obtained for steady two- and three-dimensional energy deposition in supersonic flow. We summarize several of the key results next. Linearized solutions are based on an expansion in ε with $\varepsilon \ll 1$.

1. Belokon et al. (1977)

Belokon et al. [24] considered a two-dimensional energy source of the form

$$q = q_o \exp[-(x^2 + y^2)/r_o^2] \tag{28}$$

The linearized inviscid equations were solved analytically for supersonic inflow aligned with the x axis. On the symmetry plane $y = 0$, a compression zone is formed in the energy deposition region associated with the blockage effect whereas downstream of the energy deposition region a rarefaction occurs.

2. Krasnobaev and Syunyaev (1983)

Krasnobaev and Syunyaev [25] considered a three-dimensional energy source of the form

$$q = \frac{U_\infty^3 r_o}{(x^2 + y^2 + z^2)} \tag{29}$$

The far-field linearized solution on the axis of symmetry yields a decrease in the streamwise velocity and an increase in static pressure compared with the freestream. The velocity and pressure perturbations decay proportional to z^{-1}.

3. Krasnobaev (1984)

Krasnobaev [26] extended the linearized supersonic solution to an arbitrary planar or axisymmetric confined energy source $q(r, z)$ and showed that the effect of the energy source was analogous to flow past a slender body. Krasnobaev developed the weakly nonlinear extension of the theory using the characteristic variable method of Whitham [27] to find the shape of the shock wave that forms away from the energy source.

4. Terent'eva (1992)

Terent'eva [28] further extended the linearized supersonic solution to an arbitrary confined three-dimensional energy source $q(\boldsymbol{x})$. Terent'eva derived solutions for the specific case of a finite size uniform cylindrical energy source aligned with the freestream flow given by

$$q = \begin{cases} q_o & 0 \le z \le l \quad \text{and} \quad x^2 + y^2 \le r_o^2 \\ 0 & \text{otherwise} \end{cases} \tag{30}$$

The far-field solution on the axis of symmetry yields an increase in streamwise velocity and a decrease in static pressure compared with the freestream. The dynamic pressure is decreased provided $M_\infty > \sqrt{2}$. The perturbations decay proportional to z^{-2}.

5. Vlasov et al. (1995)

Vlasov et al. [29] performed two-dimensional computations in the nonlinear regime for an energy source of the form

$$Q = \rho \frac{Q_{o_v}}{\tau_{o_v}} \exp[-(x^2 + y^2)/\ell^2] \tag{31}$$

Three qualitatively different regimes[†] were observed depending on the value of the parameter ε' (see also the related work by Georgievskii and Levin [30]). In the first regime (subcritical), the shock wave forms away from the energy source and the flow through the energy source is supersonic, as illustrated in Fig. 1 for $\varepsilon' = 1.21$ ($W_o = 15$ and $M_\infty = 3$). In the second regime (transitional), the shock wave intersects the energy source region. This was observed for $\varepsilon' = 14.5$ ($W_o = 300$ and $M_\infty = 5$). In the third regime (supercritical), the shock wave forms upstream of the energy source and intersects the axis, as illustrated in Fig. 2 for $\varepsilon' = 24.1$ ($W_o = 300$ and $M_\infty = 3$).

The appearance of the shock in the supercritical case is attributable to an effective choking of the flow due to heat addition. Consider a one-dimensional steady flow. The heat addition per unit mass required to choke the flow is [31]

$$\Delta q_c = \frac{c_p T_{t_\infty} (M_\infty^2 - 1)^2}{(\gamma + 1) M_\infty^2 [(\gamma - 1) M_\infty^2 + 2]} \tag{32}$$

We estimate the heat added per unit mass for flow on the centerline:

[†]The dimensionless parameter W_o introduced by Vlasov et al. [29] is

$$W_o = M_\infty \frac{\gamma^{3/2}}{(\gamma - 1)} \varepsilon'$$

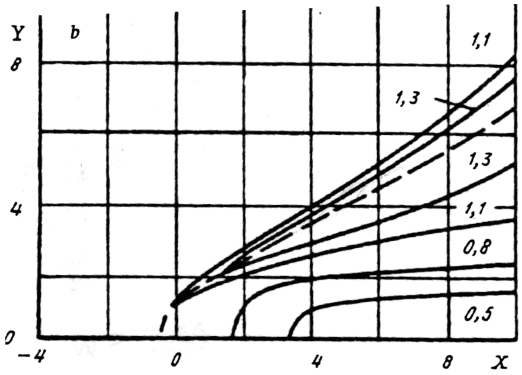

Fig. 1 Density contours (subcritical).

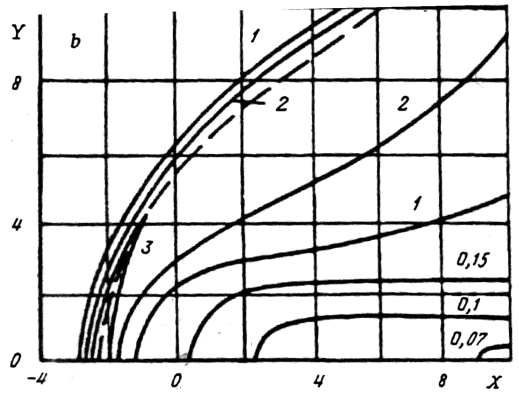

Fig. 2 Density contours (supercritical).

$$\Delta q = \int_{-\infty}^{\infty} \frac{q\,\mathrm{d}x}{u} \tag{33}$$

On the centerline, we approximate $u \approx u_s$. We define the ratio of the energy added per mass to the energy per mass required to choke the flow as

$$\varpi = \Delta q / \Delta q_c \tag{34}$$

and, thus,

$$\varpi = \frac{(\gamma^2 - 1)}{2} \sqrt{\frac{\pi}{\gamma^3}} \frac{M_\infty}{(M_\infty^2 - 1)^2} \frac{U_\infty}{u_s} W_o \tag{35}$$

For the subcritical case, $\varpi = 0.42$, whereas for the supercritical case $\varpi = 22.6$ (Table 2). This simple analysis therefore implies that the rate of energy addition in the supercritical case is sufficient to choke the flow. According to a one-dimensional steady flow analysis, it is not possible for the flow to be continuously decelerated by heat addition from supersonic to subsonic flow; therefore, a shock wave must form on the centerline as seen in Fig. 2.

6. Georgievskii and Levin (1998)

Georgievskii and Levin [32] performed a series of Euler computations at $M_\infty = 3$ for a cylindrically symmetric energy deposition:

$$Q = \rho Q_{o_g} \exp\left[-(r^2 + z^2/\ell^2)\right] \tag{36}$$

where $r^2 = x^2 + y^2$. The flowfield‡ was observed to be subcritical (i.e., supersonic everywhere) for $\varepsilon' = 1.6$, with a "hanging" shock formed outside the energy deposition region (Fig. 3). For $\varepsilon' = 8.1$, a supercritical flowfield was observed with a shock formed upstream of the energy deposition region (Fig. 4).

‡The dimensionless parameter $\hat{Q}_o$ introduced by Georgievskii and Levin [32] is identical to W_o used by Vlasov et al [29].

Table 2 Values of u_s/U_∞ from Figs. 2 and 3 of Vlasov et al. [29]

W_o	u_s/U_∞	ε	ϖ
15	≈0.85	1.21	0.42
300	≈0.32	24.1	22.6

The values of ϖ defined in Eq. (34) are shown in Table 3. The subcritical and supercritical cases correspond to $\varpi = 1.9$ and 3.9, respectively. The value of ϖ may be incorrect, however, because the value of ρ_s/ρ_∞ has been estimated. (ρ_s is the estimated value of the density at the energy source.) Nonetheless, the appearance of the shock in the upstream portion of the energy deposition region corresponds to a higher value of ϖ than in the subcritical case, thereby lending credence to the interpretation of the shock formation as attributable to the choking of the flow in the vicinity of the centerline by energy addition.

B. Unsteady Energy Deposition

1. Georgievski and Levin (1998)

Georgievski and Levin [32] performed a series of unsteady Euler simulations at $M_\infty = 3$ for a cylindrically symmetric time-dependent energy deposition of the form

$$Q = \rho Q_{o_g} \sigma(t) \exp\left[-(r^2 + z^2/r_o^2)\right] \tag{37}$$

where $r^2 = x^2 + y^2$. Results for the unsteady energy deposition (Table 4) were obtained for $\hat{Q}_o = 100$. Three different temporal variations of energy deposition were considered

$$\sigma(t) = \begin{cases} \tau_i \tau_e^{-1} & 0 \le \mathrm{mod}(t, \tau_i) < \tau_e \\ 0 & \tau_e \le \mathrm{mod}(t, \tau_i) < \tau_i - \tau_e \end{cases} \tag{38}$$

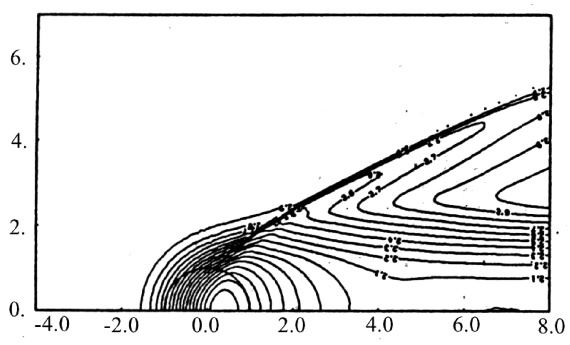

Fig. 3 Mach contours (subcritical).

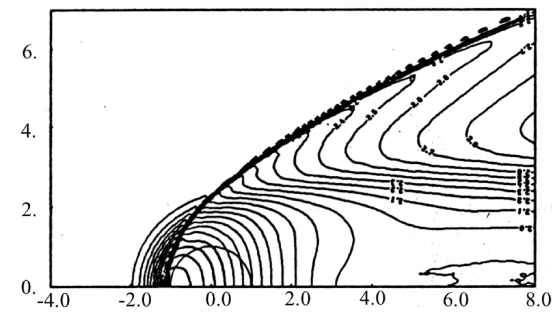

Fig. 4 Mach contours (supercritical).

Table 3 Values of ρ_s/ρ_∞ from Fig. 3 of Georgievskii and Levin [32]

$\hat{Q}_o$	ρ_s/ρ_∞	ε'	ϖ
20	≈1.0	1.6	1.9
100	≈0.4	8.1	3.9

Table 4 Georgievskii and Levin [32] (it is assumed that $\ell = 2r_o$)

$\hat{Q}_o$	$\tau_i a_\infty/\sqrt{\gamma} r_o$	δ_i	Type
100	0.3	0.54	quasi stationary
	1.2	2.13	unsteady

$$\sigma(t) = \begin{cases} \frac{1}{2}\pi\tau_i\tau_e^{-1}\sin(\pi t\tau_e^{-1}) & 0 \le \mathrm{mod}(t,\tau_i) < \tau_e \\ 0 & \tau_e \le \mathrm{mod}(t,\tau_i) < \tau_i - \tau_e \end{cases} \tag{39}$$

$$\sigma(t) = 1 + \sin(2\pi t/\tau_i) \tag{40}$$

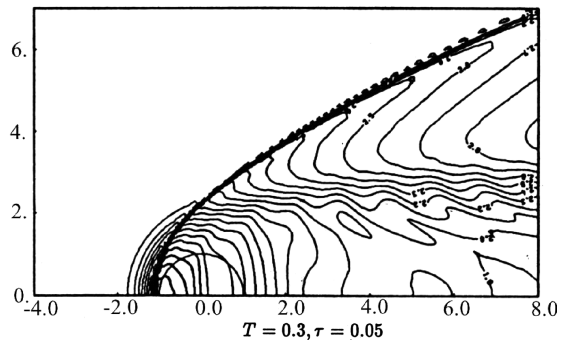

Fig. 5 Mach contours ($\delta_i = 0.53$, $\delta_e/\delta_i = 1/6$).

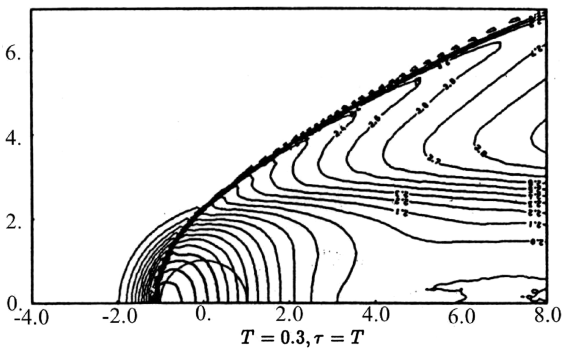

Fig. 6 Mach contours ($\delta_i = 0.53$, $\delta_e/\delta_i = 1$).

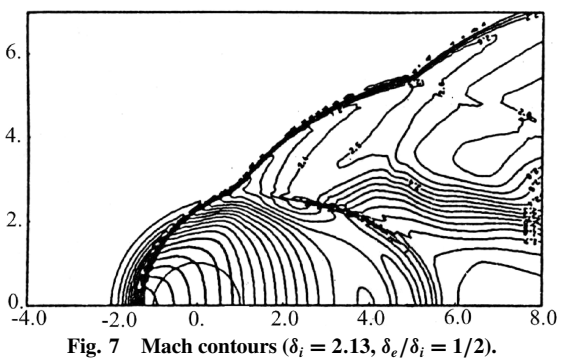

Fig. 7 Mach contours ($\delta_i = 2.13$, $\delta_e/\delta_i = 1/2$).

Equations (38–40) satisfy Eq. (8), that is, the energy deposited in the time interval τ_i is independent of the value of τ_e. Results were obtained (Table 4) for dimensionless time intervals $\delta_i = 0.54$ and 2.13 for different values of δ_e/δ_i from 1/6 to 1. For $\delta_i = 0.54$, the flow was quasi steady irrespective of the value of δ_e/δ_i, as shown in Fig. 5 ($\delta_e/\delta_i = 1/6$) and Fig. 6 ($\delta_e/\delta_i = 1$) for $\sigma(t)$ defined by Eq. (38). The behavior is expected because the energy deposition interval τ_i is approximately half the time required for the flow to transit the energy deposition region $\approx 2\ell$; thus, the energy deposition appears relatively continuous. Similar quasi-steady results were obtained at the same δ_i for $\sigma(t)$ given by Eqs. (39) and (40). For $\delta_i = 2.13$, the flow is unsteady, as shown in Fig. 7 for $\delta_e/\delta_i = 1/2$ and $\sigma(t)$ given by Eq. (38). The interval between energy pulses is larger than the flow transit time across the energy deposition region, and thus generates an unsteady sequence of shocks. The interval ratio δ_e/δ_i becomes important because the total energy deposition in time interval τ_i is the same and, hence, as τ_e/τ_i decreases, the power of the energy deposition increases and the shocks become stronger.

IV. Energy Deposition for Drag Reduction

A. Introduction

Energy deposition has been investigated as a method for controlling the aerodynamic forces and moments on air vehicles. In this paper, we focus on drag reduction. Significant additional research has been performed on the use of energy deposition for controlling lift and moments.

The efficiency of steady energy deposition for drag reduction can be examined in two limiting cases. First, consider the situation wherein the cross section of the region of energy deposition A_∞ is comparable or larger than the cross section A of the aerodynamic body. The power required to overcome the drag on the body is

$$P = \tfrac{1}{2} C_D \rho u^2 A U_\infty \tag{41}$$

where ρ and u are the effective density and velocity upstream of the body due to the energy deposition, and U_∞ is the freestream velocity. We may define the efficiency of energy deposition as

$$\eta = -\frac{\mathrm{d}P}{\mathrm{d}Q} \tag{42}$$

where $dQ = \rho_\infty U_\infty A_\infty dq$ and q is the energy added per unit mass per unit time. Because the drag coefficient C_D is relatively constant for blunt bodies in supersonic flow,

$$\frac{\mathrm{d}P}{\mathrm{d}Q} = \frac{1}{\dot{m}} \frac{C_D}{2} A U_\infty \frac{\mathrm{d}\rho u^2}{\mathrm{d}q} \tag{43}$$

where $\dot{m} = \rho_\infty U_\infty A_\infty$. For Rayleigh flow (assuming the flow is not choked),

$$\frac{\mathrm{d}\rho u^2}{\mathrm{d}q} = -\frac{\rho u^2}{(M^2 - 1) c_p T} \tag{44}$$

Approximating $T \approx T_\infty$ and $\rho \approx \rho_\infty$,

$$\eta = \frac{(\gamma - 1)}{2} C_D \frac{A}{A_\infty} \frac{M_\infty^2}{(M_\infty^2 - 1)} \tag{45}$$

Typically, $C_D \approx 1$ for blunt bodies. (For example, the drag coefficient for a sphere [33] is $0.92 \le C_D \le 1.0$ for $1.5 \le M_\infty \le 4.0$.) The foregoing analysis applies to $A_\infty \ge A$; thus, we have the estimated maximum efficiency $\eta \approx \frac{1}{2}(\gamma - 1) = 0.7$ for air. Therefore, energy deposition into a region whose cross-sectional area is comparable to the body cross-sectional area is ineffective, that is, the savings in power due to the reduction in drag is less than the power required to heat the gas.

Second, consider the situation wherein the cross section of the energy deposition A_∞ is small comparable to the cross section A of the aerodynamic body. Assume for simplicity that the energy deposition occurs at constant pressure (isobaric) and in a cylindrical

region of diameter d (a "filament") and streamwise length L aligned with the flow (with $d \ll L$ and, hence, the term filament) and initially located upstream of the blunt body. The net energy ΔE_f added in the volume $A_\infty L$ to increase the temperature from the ambient T_∞ to the level $T_f = T_\infty + \Delta T$ is

$$\Delta E_f = A_\infty L c_p \rho_f \Delta T \tag{46}$$

where ρ_f is the density of the filament. Because the energy is assumed to be added at a constant pressure,

$$\Delta E_f = A_\infty L c_p (p_\infty / R)(1 - \alpha) \tag{47}$$

where R is the gas constant for air and $\alpha = \rho_f / \rho_\infty$. During the interaction time τ of the filament with the aerodynamic body, the net energy savings ΔE_d due to decrease in frontal drag is

$$\Delta E_d = U_\infty I^* \tag{48}$$

where I^* is the impulse

$$I^* = \int_o^\tau \int_A (p - p_o)\, \mathrm{d}A\, \mathrm{d}t \tag{49}$$

where p is the instantaneous pressure on the frontal surface of the body during the interaction, p_o is the (steady) pressure on the frontal surface of the body in the absence of the interaction, and dA is the projected elemental area of the frontal surface. We define the nondimensional impulse I according to

$$I = \frac{I^*}{p_s A L U_\infty^{-1}} \tag{50}$$

where p_s is the stagnation pressure downstream of a normal shock at the freestream Mach number M_∞ (Rayleigh pitot formula). Assuming the aerodynamic body is cylindrical with diameter D, the efficiency $\eta = \Delta E_d / \Delta E_f$ is

$$\eta = \left[\frac{(\gamma+1)}{2} M_\infty^2\right]^{\gamma/(\gamma-1)} \left[\frac{\gamma+1}{2\gamma M_\infty^2 - (\gamma-1)}\right]^{1/(\gamma-1)} \frac{(\gamma-1)}{\gamma} \times \left(\frac{D}{d}\right)^2 \frac{I}{(1-\alpha)} \tag{51}$$

For $M_\infty \gg 1$,

$$\eta \sim 0.37 M_\infty^2 (D/d)^2 (I/(1-\alpha)) \tag{52}$$

Unlike the first situation, the efficiency improves both with increasing Mach number M_∞ and area ratio (D/d). Indeed, if we conjecture that the impulse I is relatively insensitive to (D/d), the efficiency increases dramatically with decreasing filament diameter. Numerical simulations [34] confirm this conjecture. Numerical experiments were performed by Kremeyer et al. [35] for energy deposition along a finite length upstream of a cone at supersonic speeds and zero angle of attack. The instantaneous energy deposition generated a cylindrical shock wave [36] and a low-density heated core. The interaction of the heated filament with the cone cylinder resulted in a drag reduction of up to 96%.

B. Steady Energy Deposition

1. *Georgievskii and Levin (1991)*

Georgievskii and Levin [30] considered the effect of a steady energy deposition upstream of a body of revolution in supersonic flow at zero angle of attack for two different cases. In the first case, the energy deposition was assumed to occur on an infinitesimally thin line parallel to the flow and upstream of the body as shown in Fig. 8. The linearized problem was solved and a general expression for the drag coefficient was obtained. Specific results were presented for a shape consisting of a conical forebody and afterbody of equal length. It was shown that a net thrust can be achieved. The shape of the body of revolution of a given volume and minimum resistance was determined analytically.

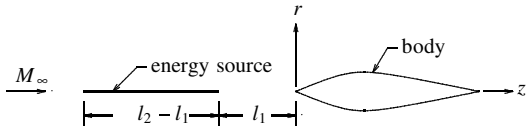

Fig. 8 Energy deposition on line.

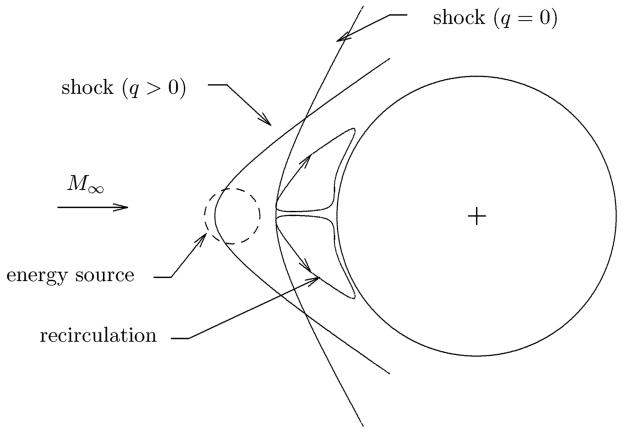

Fig. 9 Recirculation region.

In the second case, a Gaussian energy deposition was assumed upstream of the body of the form

$$q = \frac{Q_{o_s}}{R_o} \left(\frac{p_\infty}{\rho_\infty}\right)^{3/2} \exp\left[-\left(\frac{r^2 + (z - z_o)^2}{r_o^2}\right)\right] \tag{53}$$

where r_o is the effective scale of the energy deposition, R_o is the characteristics dimension of the body, and $r^2 = x^2 + y^2$. For a sufficiently large energy deposition, a recirculation region forms in front of the body, as shown in Fig. 9. The formation of a recirculation region in front of a bluff body in the presence of intense upstream energy deposition was also observed by Artem'ev et al. [37], Borzov et al. [38], and Georgievskii and Levin [39,40]. A reduction in drag (i.e., integrated frontal surface pressure) was observed for sufficiently high levels of energy deposition. The magnitude of the drag reduction was found to be insensitive to the location of energy deposition at a sufficiently large distance from the body. This phenomenon was denoted "distance stabilization." Also, the increment in drag reduction diminished with increasing energy addition.

2. *Levin and Terent'eva (1993)*

Levin and Terent'eva [41] considered steady symmetric energy deposition upstream of a cone in supersonic flow at zero angle of attack. The energy release was assumed to be Gaussian (53). Numerical simulations of the Euler equations were performed for the following ranges of values: 1) $M_\infty = 3$–4.25, 2) cone half-angles of

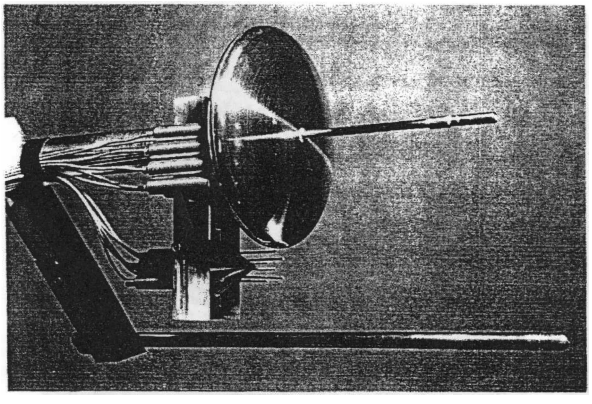

Fig. 10 Directed air spike.

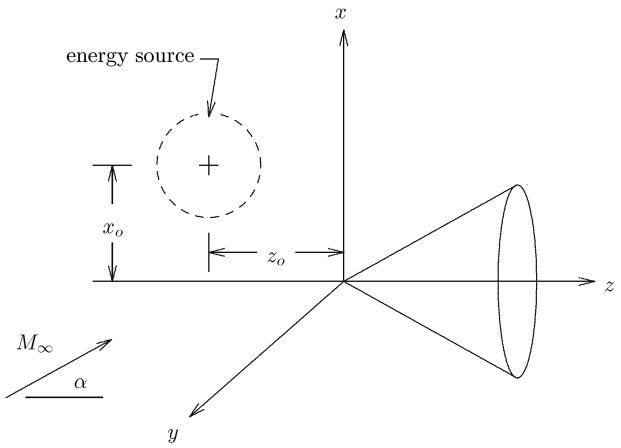

Fig. 11 Flow configuration.

$\theta = 10$–25 deg, 3) energy deposition ε, and 4) energy locations z_o. The frontal drag was reduced for the range of cone angles studied by up to 45%. However, for sufficiently long cones, the shock generated by the energy release interacted with the cone shock and an increased drag occurred. The position of the energy release for minimum drag with a fixed energy deposition q and M_∞ was determined.

3. Toro et al. (1998)

Toro et al. [42] performed a series of experiments for a "directed air energy spike" based on the concepts of Myrabo and Raizer [43]. The experimental model is shown in Fig. 10. The model body is a double 15.2 cm disk whose surfaces are scaled directly from the Apollo command module's lower heat shield. A 15.2 cm long plasma torch with a 0.635 cm external diameter is attached on the model centerline. Experiments were performed at $M_\infty = 10$. Operation of the plasma torch at arc powers up to 70 kW resulted in a reduced frontal drag compared with the power-off drag with the torch body attached. Additional experiments and axisymmetric Euler computations were performed for this configuration by Bracken et al. [44,45].

4. Levin and Terent'eva (1999)

Levin and Terent'eva [46] considered steady asymmetric energy deposition upstream of a cone in supersonic flow at small angles of attack. The configuration is shown in Fig. 11. The energy release is Gaussian with the form

$$q = q_o \exp\left[-\left(\frac{(x-x_o)^2 + (z-z_o)^2}{l^2}\right)\right] \tag{54}$$

Euler simulations were performed for supersonic flow at cone half-angles θ from 5 to 15 deg and angles of attack α from 0 to 10 deg. It was observed that the energy deposition located upstream and above the cone centerline both reduced the drag and increased the lift at positive α.

5. Riggins et al. (1999, 2000)

Riggins et al. [47] and Riggins and Nelson [48] performed a series of laminar viscous computations of steady energy deposition upstream of a 2-D/axisymmetric semicircle/hemisphere cylinder at $M_\infty = 6.5$ and 10. The formation of two counter-rotating vortices (2-D) or an annular vortex (axisymmetric) was observed [i.e., recirculation region(s)]. They defined a power effectiveness according to

$$\mathcal{E} = \frac{(D_{q=0} - D_{q>0})U_\infty}{Q} \tag{55}$$

where $D_{q=0}$ is the drag in the absence of energy deposition, $D_{q>0}$ is the drag in the presence of energy deposition, and Q is the total energy added per unit time. The computed $\mathcal{E}$ exceeded 1 for all cases considered. Wave drag reduction of up to 50% was observed.

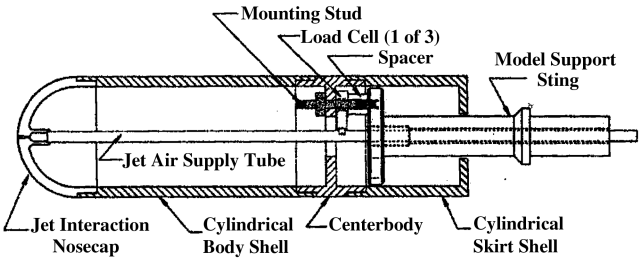

Fig. 12 Flow configuration.

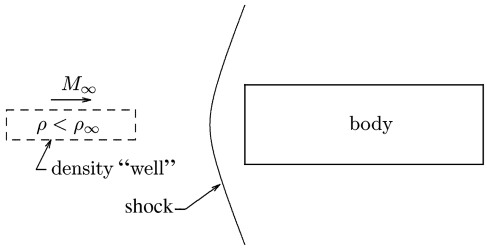

Fig. 13 Initial condition for energy pulse.

6. Shang et al. (2001)

Shang et al. [49] considered a plasma counterjet issuing from a hemisphere cylinder at $M_\infty = 5.8$. Both experiments and computations were performed. The configuration is shown in Fig. 12. At a constant counterjet mass flow rate, a decrease in drag was observed with increasing counterjet temperature. A maximum drag reduction of 13% was achieved. The possible plasmadynamic contribution to the drag reduction was not quantified.

7. Yuriev et al. (2001)

Yuriev et al. [77] considered steady energy deposition near the surface of an NACA 0012 airfoil for $0.8 \leq M_\infty \leq 0.9$. Euler simulations indicated that energy deposition can reduce profile drag up to 25%, depending on the location of the energy deposition.

8. Kolesnichenko et al. (2002)

Kolesnichenko et al. [34] considered both quasi-steady and unsteady energy deposition upstream of a 2-D rectangular body. Euler simulations were performed for a series of energy pulses at $M_\infty = 1.9$ defined by an initial condition comprised of a finite rectangular region upstream of the body with $\rho < \rho_\infty$ but $p = p_\infty$ and $u = U_\infty$, as shown in Fig. 13. They observed that quasi-static energy deposition was more efficient than unsteady energy deposition in reducing the time integrated frontal drag. The strongest effect on drag reduction was the magnitude of the density "well" (i.e., the magnitude of $\rho_\infty - \rho$ in the initial energy pulse). They noted that the interaction of the density well with the bow shock produced a

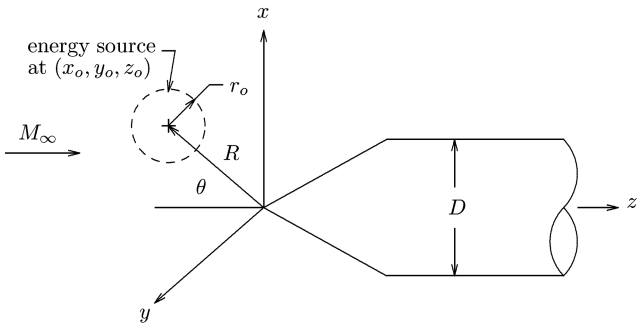

Fig. 14 Flow configuration.

vortex pair, which is associated with the reduced pressure on the front surface (and, hence, reduced drag). This is consistent with previous investigations that showed recirculation regions in front of blunt bodies in the presence of energy deposition. They also noted that the integrated effect of the density well was independent of its transverse dimension.

9. Girgis et al. (2002)

Girgis et al. [50] considered steady energy deposition upstream of a cone cylinder (Fig. 14). Euler simulations were performed for a 15 deg half-angle cone at $M_\infty = 2.4$–5 and zero angle of attack and sideslip. The energy deposition was assumed Gaussian of the form

$$Q = Q_o \exp\left[-\left(\frac{(x-x_o)^2 + (y-y_o)^2 + (z-z_o)^2}{\ell^2}\right)\right] \tag{56}$$

Two studies were conducted to assess the effect of the size and location of the energy deposition on drag. In both studies, the energy source was located on the axis ($\theta = 0$ in Fig. 14) and $Q_t = \frac{1}{2}\rho_\infty U_\infty^3 A$ where Q_t is the total energy added per unit time and $A = \pi D^2/4$ is the cross-sectional area of the cylinder. (This quantity is proportional to the ratio of the total energy added per unit time to the power required to overcome the drag on the cone cylinder at fixed M_∞.) In the first study, the effect of the location of the energy deposition was examined. The effective radius of the energy deposition was assumed to be $\ell = 0.2D$ where D is the diameter of the cylinder. The location of the center of the energy deposition was varied from $R/D = 0.04$ to 1.75. The minimum drag occurred at $R/D = 0.4$. At this location, a drag reduction of 35% was achieved. In the second study, the effective radius ℓ of the energy source was varied from $\ell/D = 0.15$ to 0.4. Note that the energy deposition is more intense as ℓ/D decreases. The minimum drag corresponds to $\ell/D = 0.15$; however, this may not represent the global minimal drag under the conditions of this study because computation at smaller ℓ/D was infeasible due to the limitations of the computational grid used. A drag reduction of 35% was obtained.

10. Georgievskii and Levin (2003)

Georgievskii and Levin [51] examined the effect of the relative size of the energy deposition region on the drag of blunt and cone–cylinder bodies. Numerical simulations were performed for Mach 2–10 at different energy deposition levels and with ellipsoidal energy deposition shapes of different aspect ratios with one axis aligned with the axis of symmetry of the body. A "continuous flow deceleration" regime was identified wherein the flow Mach number decreased continuously to subsonic values without shock formation on the axis. This regime allowed an efficient drag reduction for cone–cylinder (i.e., streamlined) bodies.

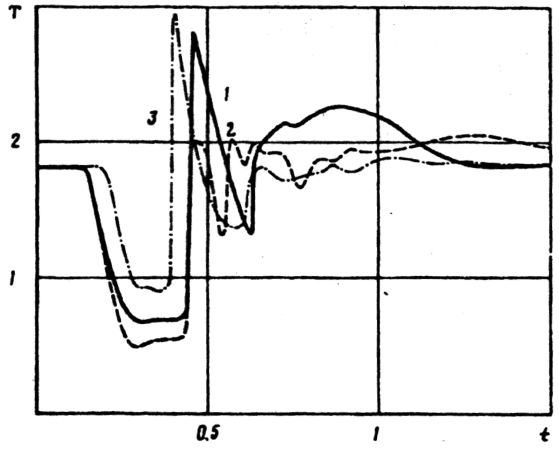

Fig. 15 Temperature vs time.

C. Unsteady Energy Deposition

1. Georgievskii and Levin (1993, 2004)

Georgievskii and Levin [52] performed a series of Euler simulations at $M_\infty = 3$ for the interaction of a thermal spot of various configurations with a sphere. The thermal spot originated upstream of the blunt body shock and was defined by a region of uniform reduced density ρ_s of the shape

$$(r/\alpha_r r_o)^2 + (z/\alpha_z r_o)^2 \le 1 \tag{57}$$

where r_o is the radius of the sphere, and α_r and α_z are dimensionless constants. The parameters $(\alpha_r, \alpha_z) = (0.5, 0.5)$, $(0.5, \infty)$, $(0.3, 0.3)$, $(0.6, 0.3)$, and $(0.15, 0.3)$ were considered. The pressure and velocity within the initial thermal spot was set equal to freestream values.

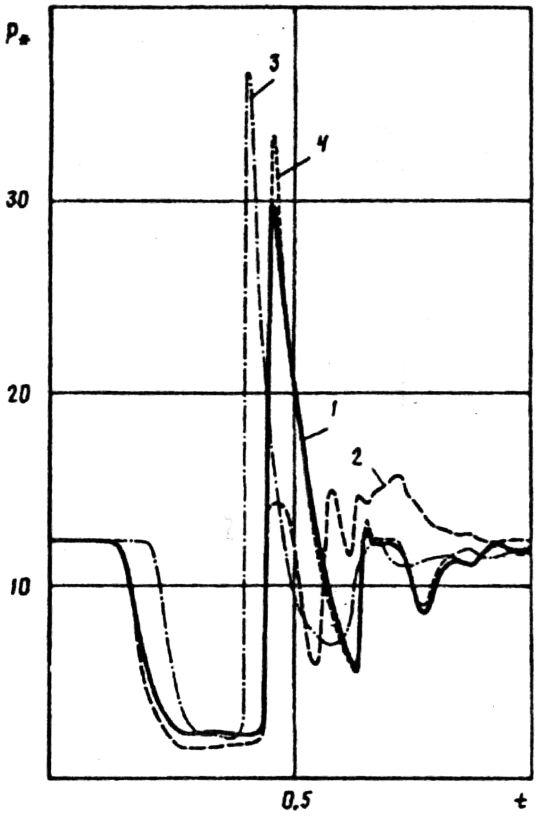

Fig. 16 Pressure vs time.

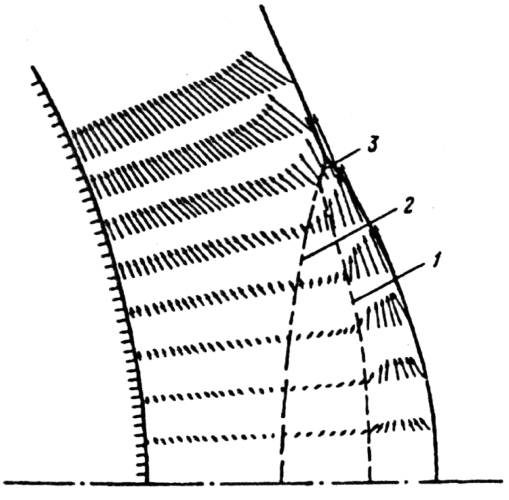

Fig. 17 Flowfield structure.

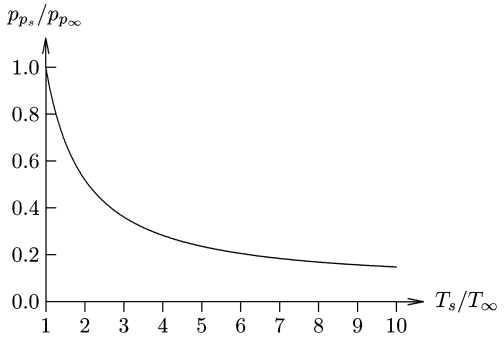

Fig. 18 Pitot pressure vs T_s/T_∞ at $M_\infty = 3$.

Results are shown for $\rho_s/\rho_\infty = 0.2$ for the first through third (fourth) sets of values of (α_r, α_z) in Figs. 15 and 16 for the temperature and pressure at the stagnation point on the sphere vs time. An instantaneous image of the velocity vectors is shown in Fig. 17. The initial interaction of the thermal spot with the blunt body shock causes a "lensing" of the shock (i.e., upstream motion of the shock) due to the reduced Mach number of the spot associated with its increased temperature (Fig. 17). A similar effect was observed by Aleksandrov et al. [53]. In addition, the interaction of the thermal spot with the blunt body shock causes an expansion wave to propagate toward the surface of the sphere, as indicated by curve 2 in Fig. 17. The expansion wave reaches the surface and causes a decrease in temperature and pressure at the stagnation point, as seen in Figs. 15 and 16. The fluid within the thermal spot is turned along the shock, because the stagnation pressure of the thermal spot fluid upon traversing the blunt body shock is lower than the stagnation pressure of the freestream flow that has preceded it. This is shown quantitatively in Fig. 18, which displays the computed ratio[§] of the pitot pressure (i.e., the stagnation pressure downstream of a normal shock) for the thermal spot to the pitot pressure for the freestream flow vs the ratio of the upstream static temperature in the thermal spot to the freestream static pressure at $M_\infty = 3$ and $\gamma = 1.4$. The leading boundary of the thermal spot is shown as curve 1 in Fig. 17. After the thermal spot has convected through the shock, a higher pressure and density are achieved behind the shock wave associated with the freestream flow. A compression wave thereupon forms and moves to the sphere surface causing an increase in surface temperature and pressure (Figs. 15 and 16). The exact details of the surface temperature and pressure depend upon the thermal spot shape, but qualitatively the behavior is similar for all cases.

Georgievskii and Levin [54] performed a series of axisymmetric Euler simulations at Mach 2 for pulse-periodic energy deposition upstream of a sphere, ogive body, and cone cylinder. The results demonstrate a significant reduction in drag for all configurations and the capability of achieving virtually the same results as stationary energy deposition for a sufficiently high frequency of energy deposition. Results for pulse-periodic energy deposition upstream of a 25 deg cone are shown in Fig. 19.

2. Tretyakov et al. (1996)

Tretyakov et al. [55] (also see Tretyakov et al. [56]) performed experiments to measure the drag on a cone cylinder and hemisphere cylinder at $M_\infty = 2$ in argon in the presence of a high frequency CO_2 laser discharge upstream of the body. Results were obtained for focal locations at one and two diameters upstream of the body on the centerline. The relevant dimensionless pulse interval is δ_L. The time

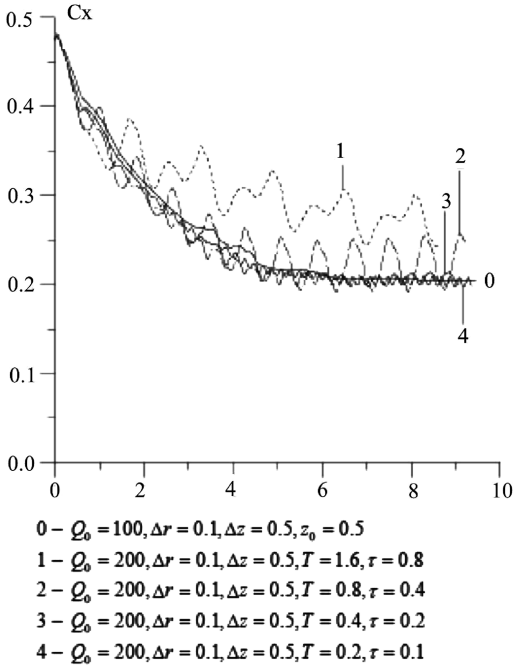

0 – $Q_0 = 100, \Delta r = 0.1, \Delta z = 0.5, z_0 = 0.5$
1 – $Q_0 = 200, \Delta r = 0.1, \Delta z = 0.5, T = 1.6, \tau = 0.8$
2 – $Q_0 = 200, \Delta r = 0.1, \Delta z = 0.5, T = 0.8, \tau = 0.4$
3 – $Q_0 = 200, \Delta r = 0.1, \Delta z = 0.5, T = 0.4, \tau = 0.2$
4 – $Q_0 = 200, \Delta r = 0.1, \Delta z = 0.5, T = 0.2, \tau = 0.1$

Fig. 19 Drag coefficient.

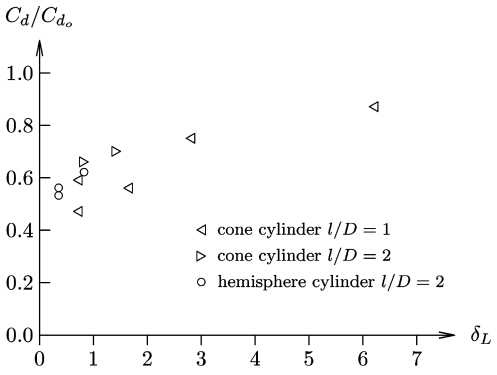

Fig. 20 Drag coefficient vs δ_L.

average drag is reduced by up to 45% for $\delta_L \approx 1$, as indicated in Fig. 20 in which D is the diameter of the cylinder. As $\delta_L \to 0$, the pulsed energy deposition acts like a quasi-steady source of energy upstream of the flow. It is well known [30,40,46,47,57] that steady energy deposition upstream of a blunt body reduces the drag due to the reduction in ρu^2 with heat addition.

3. Adelgren et al. (2001, 2002)

Adelgren et al. [58–60] examined the effect of pulsed energy deposition on the flow past a sphere at $M_\infty = 3.45$. A Nd:YAG laser (532 nm, 10 ns pulse duration, 10 Hz repetition rate) was used in all experiments with energy levels from 12 to 300 mJ. The first configuration is an isolated sphere. A single laser pulse generates a thermal spot upstream of the bow shock. The interaction of the thermal spot with the bow shock is shown in Fig. 21. The bow shock initially lenses forward (Figs. 21a and 21b). Subsequent compression waves form (Fig. 21c) as the thermal spot is convected downstream (Fig. 21d). The temporal behavior of the surface pressure on the centerline is shown in Fig. 22 for energy pulses of 13, 127, and 258 mJ. The ordinate is the stagnation pressure on the centerline normalized by its undisturbed value. The initial pressure rise is associated with the interaction of the blast wave with the sphere. The interaction of the thermal spot with the bow shock generates an expansion wave. Upon completion of the passage of the thermal spot

[§]The ratio is

$$\frac{p_{p_s}}{p_{p_\infty}} = \left[\frac{T_\infty}{T_s}\right]^{\gamma/(\gamma-1)} \left[\frac{2\gamma M_\infty^2 - (\gamma-1)}{2\gamma M_\infty^2 T_\infty/T_s - (\gamma-1)}\right]^{1/(\gamma-1)}$$

where p_{p_s} is the pitot pressure of the thermal spot downstream of a normal shock, p_{p_∞} is the pitot pressure of the freestream flow downstream of a normal shock, and T_s and T_∞ are the static temperatures of the thermal spot and freestream upstream of the normal shock, respectively.

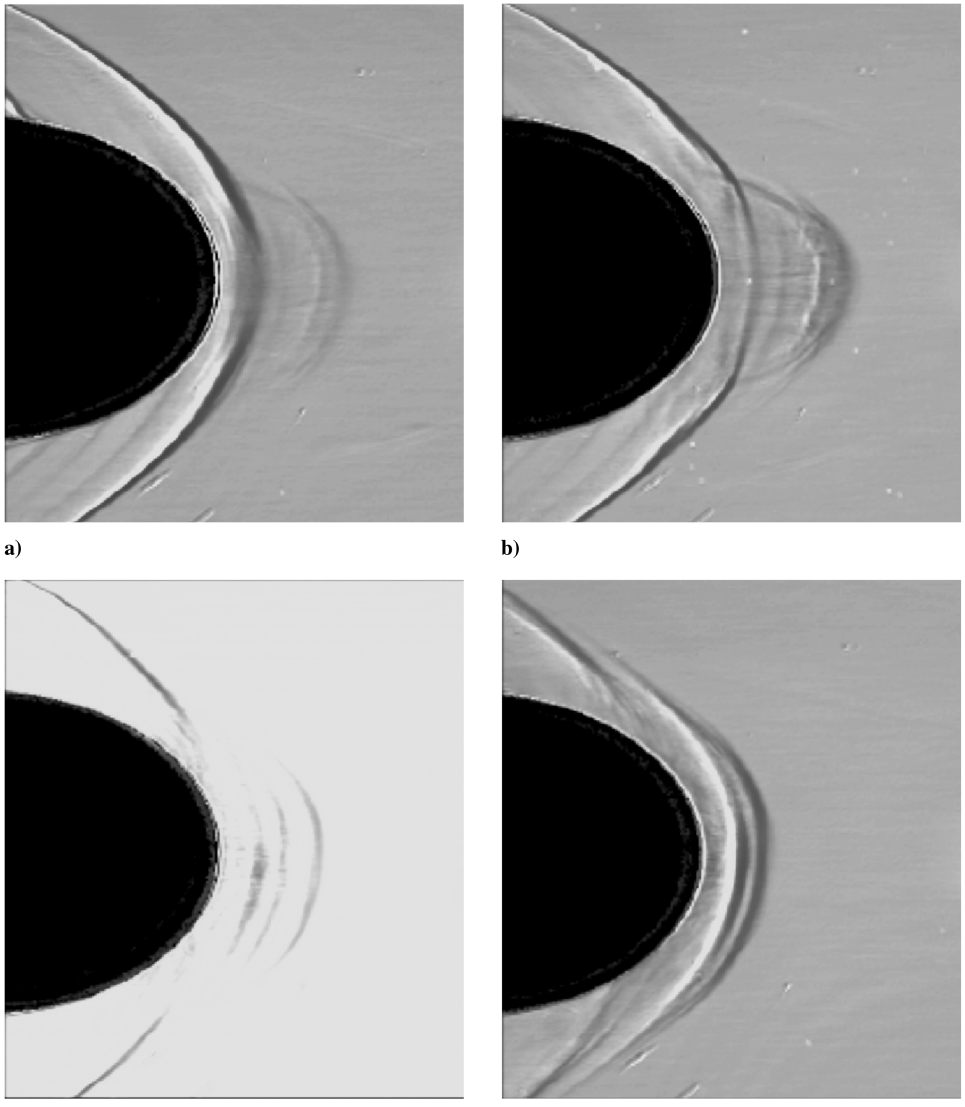

Fig. 21 Laser energy deposition.

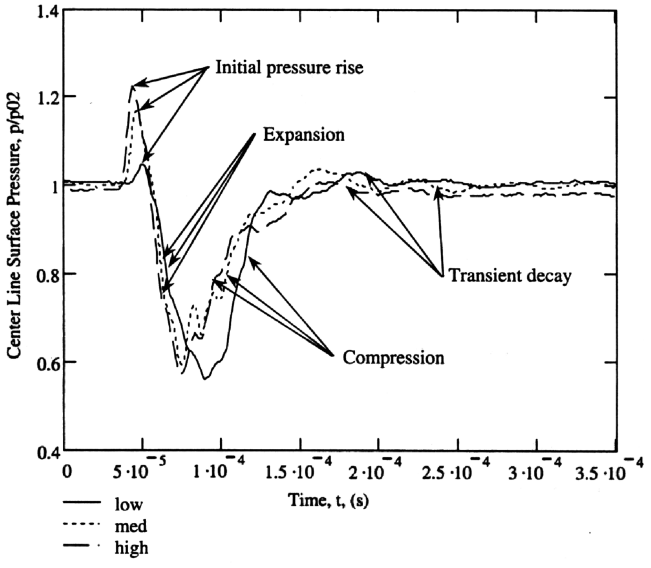

Fig. 22 Stagnation pressure vs time.

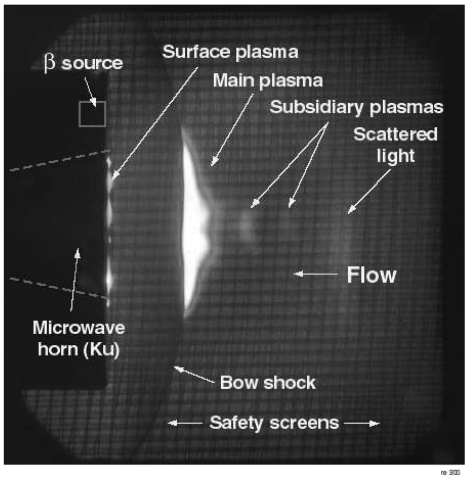

Fig. 23 Schlieren image.

through the bow shock, a compression wave forms and the surface pressure recovers to its undisturbed value.

4. Exton et al. (2001)

Exton et al. [61] conducted an experiment with microwave energy deposition in a Mach 6 flow past a blunt cylinder (diameter $D = 8.26$ cm) containing a Ku-band (16.5 GHz) microwave horn and a ^{90}Sr initiator. Square-wave microwave pulses with a power $P = 475$ kW and pulse duration of 3.5 μs were used. Two different freestream stagnation conditions were examined corresponding to $\varepsilon = 0.5$ and 2.0 assuming $L = D$. The pulse repetition rate was 100 Hz; consequently, there was no interaction between individual pulses. A time-averaged schlieren image is shown in Fig. 23. The main microwave discharge is focused just upstream of the shock wave and has no apparent effect on the shock standoff distance. The main plasma becomes reflective to microwave radiation during the early stages of the microwave pulse due to the increase in the electron concentration, thereby creating an effective plasma mirror. A sequence of schlieren images displays a shock originating at the surface plasma, propagating to the bow shock, and reflected back to the model surface.

5. Kolesnichenko et al. (2001, 2002, 2003, 2004)

Kolesnichenko et al. [34,62–67] examined the effect of a microwave filament discharge on the aerodynamic drag of blunt bodies at $M_\infty = 1.7$–2.1 in air, argon, carbon dioxide, and nitrogen. Typical peak microwave power was 220 kW at a maximum pulse duration of 2 μs. Detailed spectral measurements of the plasma generated by the microwave pulse were performed and analyzed using a kinetic model. Schlieren visualization displayed the typical lensing of the blunt body shock due to the interaction with the thermal spot generated by the microwave pulse. Surface pressure

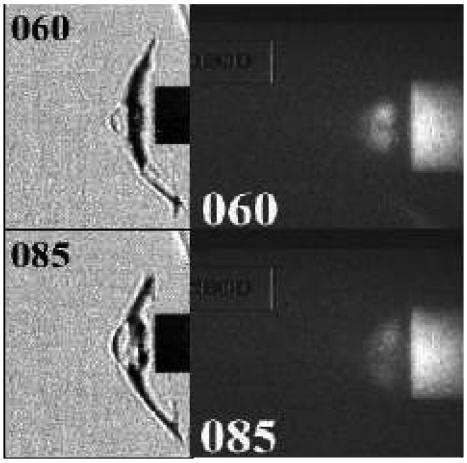

Fig. 24 Interaction of microwave filament with blunt body (left: schlieren, right: chemiluminescence).

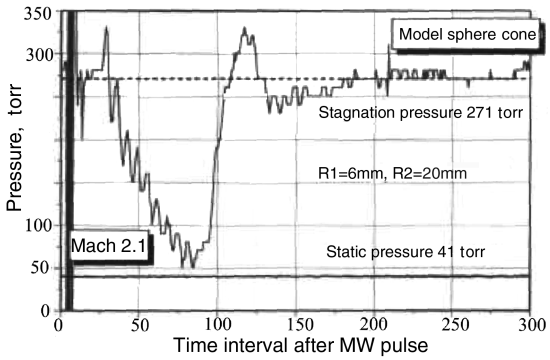

Fig. 25 Stagnation pressure vs time.

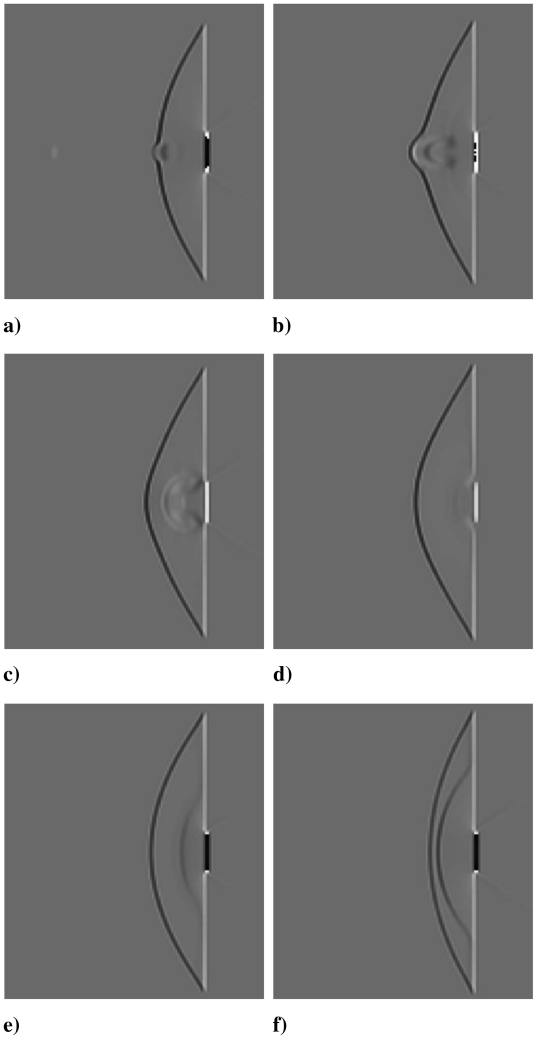

Fig. 26 Numerical schlieren images.

measurements displayed the initial drop in stagnation pressure associated with the expansion fan generated by the interaction of the thermal spot with the blunt body shock. An instantaneous schlieren image (Fig. 24, left) displays the lensing of the blunt body shock associated with the interaction of the region heated by the microwave pulse (Fig. 24, right) with the blunt body shock. Stagnation pressure measurements (Fig. 25) indicate a significant momentary drag reduction.

Kolesnichenko et al. [34] presented two-dimensional Euler simulations for quasi-static and impulsive energy deposition upstream of a rectangular body at $M_\infty = 1.9$. A sequence of numerical schlieren images are shown in Fig. 26 for the interaction of a rectangular "density well" (thermal spot) with $T_s/T_\infty = 2$ (where

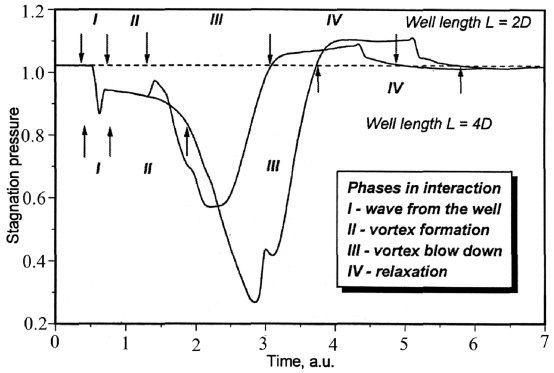

Fig. 27 Stagnation pressure vs time.

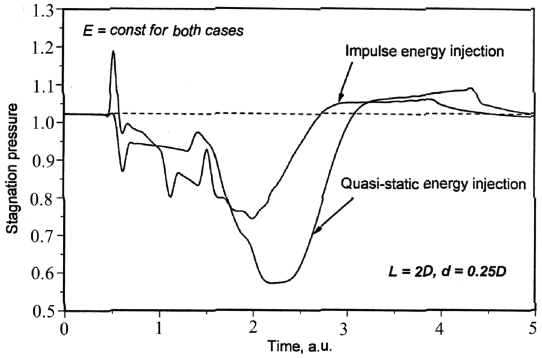

Fig. 28 Stagnation pressure vs time.

T_s is the initial static temperature in the thermal spot) with length $L = 3D$ and height $H = 0.25D$ where D is the transverse dimension of the rectangular body. The interaction of the thermal spot with the blunt body shock causes a lensing of the blunt body shock (Fig. 26a) and the formation of a vortex pair (Fig. 26b) that impinges on the blunt body surface (Figs. 26c and 26d). Upon passage of the vortex pair, a shock wave forms and propagates upstream (Figs. 26e and 26f). The time history of the stagnation pressure on the blunt body is shown in Fig. 27 and illustrates the effect of the length of the thermal spot. The initial pressure drop depends only upon the temperature ratio of the thermal spot (i.e., the ratio of the thermal spot static temperature to the freestream static temperature), whereas the final minimum pressure level depends upon the length of the thermal spot. An increase in the longitudinal dimension of the thermal spot results in an increase in the drag reduction. A comparison of an impulsive energy injection vs a quasi-static energy deposition is shown in Fig. 28, in which the same energy deposition is applied to each case. The initial rise in stagnation pressure for the impulsive energy deposition is associated with the blast wave generated by the energy deposition. The quasi-static energy deposition is more effective in reducing the stagnation pressure than the impulsive energy deposition. Figure 29 illustrates the variation in forebody drag associated with quasi-static energy deposition with different cross-stream heights and same lengths for $T_s = 2T_\infty$. Although the time history of the drag force varies between the two cases, the temporally integrated drag reduction is nearly the same for the two cases.

Azarova et al. [68] described a series of two-dimensional and axisymmetric Euler simulations of energy release in a longitudinal channel upstream of wedge-shaped bodies at Mach 1.89 (Fig. 30).

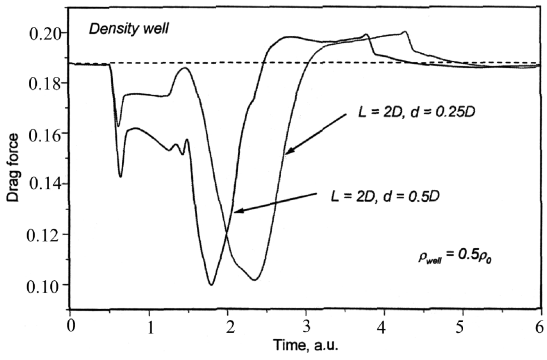

Fig. 29 Drag force vs time.

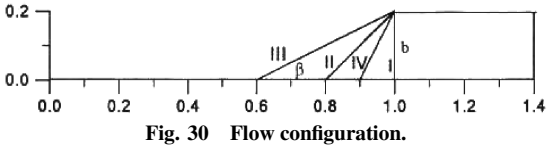

Fig. 30 Flow configuration.

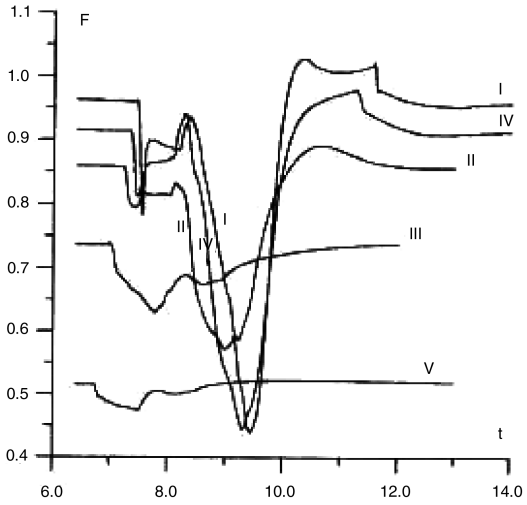

Fig. 31 Drag vs time.

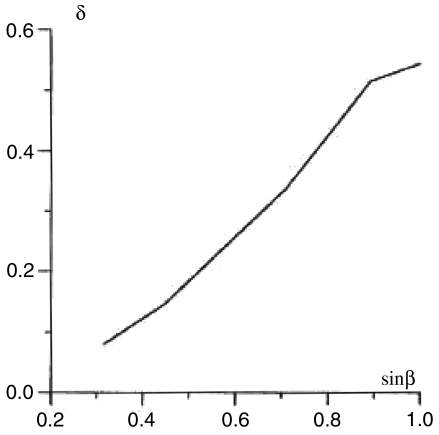

Fig. 32 Dependence of drag reduction on wedge angle.

Drag reduction was observed in all cases with the maximum effect for the blunt body (Fig. 31). The maximum relative instantaneous drag decrease $\delta = (D_{\text{steady}} - D_{\min})/D_{\text{steady}}$ was observed to vary nearly linearly with $\sin\beta$ where β is the wedge angle (Fig. 32). Details of the flowfield including the formation of vortices and their relationship to the drag reduction were discussed.

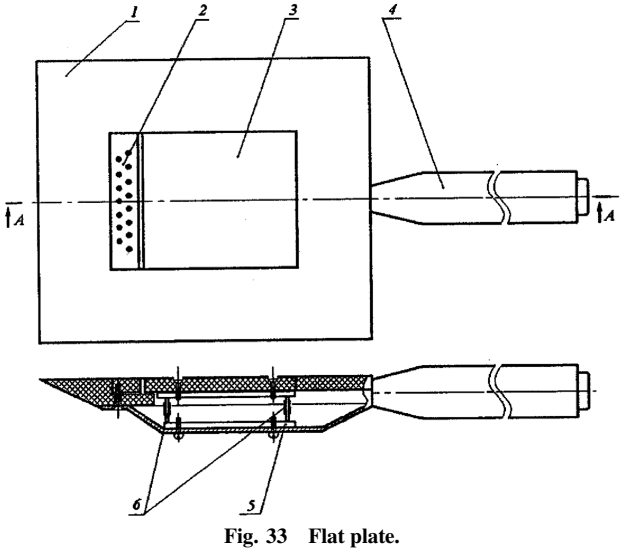

Fig. 33 Flat plate.

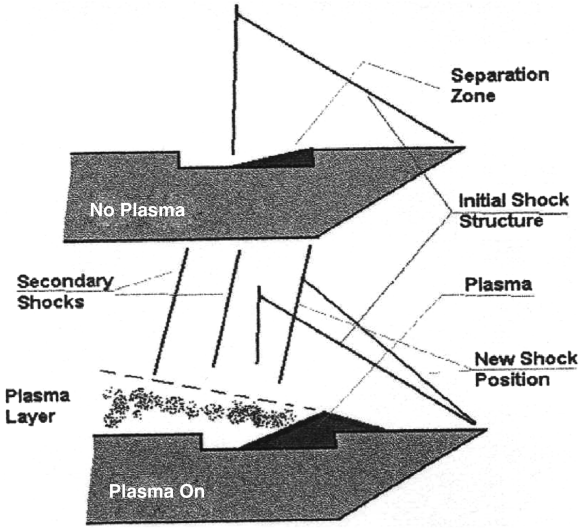

Fig. 34 Flat plate.

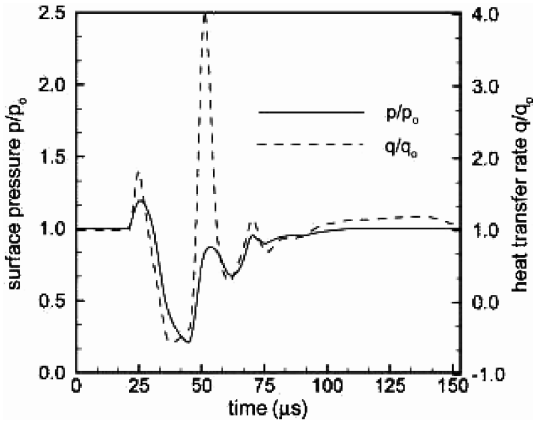

Fig. 35 Peak surface pressure and heat transfer.

6. Leonov et al. (2001, 2002)

Leonov et al. [69,70] performed a series of experiments to investigate the effect of surface electrical discharge on flow properties at transonic speeds. Figure 33 shows the surface electrodes and flat plate force balance used to evaluate the effect of surface discharge on skin friction drag at $M_\infty = 0.95$. The electrical discharge created a surface plasma that formed a subsonic heated zone near the surface. A friction drag reduction of 15–20% was measured and confirmed by simulations. Figure 34 displays the experimental configuration for energy deposition in the vicinity of a cavity. A drag force reduction of up to 40% was measured in the presence of the electrical discharge.

7. Zaidi et al. (2002)

Zaidi et al. [71] examined the effect of a single laser pulse on the structure of an oblique shock wave generated by a 10 deg half-angle wedge at $M_\infty = 2.4$ in a combined computational and experimental study. The energy deposition was modeled as an instantaneous pulse with Gaussian behavior $e^{-(r/r_o)^2}$. Shadowgraph images were obtained at a 500 kHz framing rate and showed the initial blast wave, its interaction with the wedge shock and wedge surface, and the distortion of the shock due to the passage of the thermal spot.

8. Kandala and Candler (2004)

Kandala and Candler [72] performed a computational study of the effect of a single Nd:YAG laser pulse (160 mJ, 10 ns) on the drag on a sphere at Mach 3.45. An 11-species thermochemical model of air was used together with a radiation model for energy deposition by laser pulse. The model was validated by comparison with experimental data for laser energy deposition in quiescent air. The computed peak surface pressure (Fig. 35) displays an initial rise associated with the interaction of the blast wave (generated by the laser pulse) with the sphere. A subsequent decrease in peak pressure due to the expansion wave generated by the interaction of the thermal region with the shock is clearly evident, with the peak pressure dropping by 80%, thereby confirming the capability for drag reduction. The computed heat transfer shows a similar decrease, followed by a rapid spike due to the impingement of the hot gas to the sphere.

V. Conclusions

Steady and unsteady energy deposition has been demonstrated in both experiments and ideal gas simulations to provide significant drag reduction in supersonic flows through modification of the flowfield structure. However, two major issues require further investigation. First, the effect of nonideal gas behavior in the simulations has not been examined to any significant extent. Recent results [72,73] suggest that real gas effects (e.g., dissociation of O_2) can be important. A detailed comparison of ideal vs real gas simulations for the prediction of drag reduction in canonical configurations is needed. Second, the practical application of energy deposition for drag reduction requires a detailed systems analysis taking into consideration the efficiency of energy deposition, size and weight of energy deposition devices, and control systems. Recent papers have focused on these important issues [74–76].

Acknowledgment

This research is supported by the U.S. Air Force Office of Scientific Research (AFOSR) under AFOSR grant F-49620-01-1-0368, monitored by John Schmisseur.

References

[1] *1st Weakly Ionized Gases Workshop, US Air Force Academy*, AIAA, Reston, VA, June 1997.
[2] Bain, L. (ed.), *AIAA 2nd Weakly Ionized Gases Workshop*, AIAA, Reston, VA, Nov. 1998.
[3] *AIAA 3rd Weakly Ionized Gases Workshop*,AIAA, Reston, VA, Nov. 1999.
[4] *AIAA 4th Weakly Ionized Gases Workshop*, AIAA, Reston, VA, June 2001.
[5] *AIAA 5th Weakly Ionized Gases Workshop*, AIAA, Reston, VA, Jan. 2003.
[6] *AIAA 6th Weakly Ionized Gases Workshop*, AIAA, Reston, VA, Jan. 2004.
[7] *AIAA 7th Weakly Ionized Gases Workshop*, AIAA, Reston, VA, Jan. 2005.
[8] *AIAA 8th Weakly Ionized Gases Workshop*, AIAA, Reston, VA, Jan. 2006.
[9] Kuranov, A. (ed.), "*First Workshop on Thermochemical Processes in Plasma Aerodynamics*," Hypersonic System Research Inst., Leninetz Holding Company, St. Petersburg, Russia, 2000.
[10] Kuranov, A. (ed.), "*Second Workshop on Thermochemical Processes in Plasma Aerodynamics*," Hypersonic System Research Inst., Leninetz Holding Company, St. Petersburg, Russia, Sept. 2001.
[11] Kuranov, A. (ed.), "*Third Workshop on Thermochemical and Plasma Processes in Aerodynamics*," Hypersonic System Research Inst., Leninetz Holding Company, St. Petersburg, Russia, July 2003.
[12] Kuranov, A. (ed.), "*Fourth Workshop on Thermochemical and Plasma Processes in Aerodynamics*," Hypersonic System Research Inst., Leninetz Holding Company, St. Petersburg, Russia, June 2006.
[13] Bityurin, V. (ed.), "*Perspectives of MHD and Plasma Technologies in Aerospace Applications*," Inst. for High Temperatures, Russian Academy of Sciences, Moscow, March 1999.
[14] Bityurin, V. (ed.), "*The Second Workshop on Magneto-Plasma-Aerodynamics in Aerospace Applications*," Inst. for High Temperatures, Russian Academy of Sciences, Moscow, April 2000.
[15] Bityurin, V. (ed.), "*The Third Workshop on Magneto-Plasma-Aerodynamics in Aerospace Applications*," Inst. for High Temperatures, Russian Academy of Sciences, Moscow, April 2001.

[16] Bityurin, V. (ed.), "*The Fourth Workshop on Magneto-Plasma-Aerodynamics in Aerospace Applications*," Inst. for High Temperatures, Russian Academy of Sciences, Moscow, April 2002.
[17] Bityurin, V. (ed.), "*The Fifth Workshop on Magneto-Plasma-Aerodynamics in Aerospace Applications*," Inst. for High Temperatures, Russian Academy of Sciences, Moscow, April 2003.
[18] Bityurin, V. (ed.), "*The Fifteenth International Conference on MHD Energy Conversion and Sixth Workshop on Magneto-Plasma-Aerodynamics in Aerospace Applications*," Inst. for High Temperatures, Russian Academy of Sciences, Moscow, May 2005.
[19] Bityurin, V. (ed.), "*Seventh Workshop on Magneto-Plasma Aerodynamics*," Inst. for High Temperatures, Russian Academy of Sciences, Moscow, April 2007.
[20] Zheltovodov, A., *Development of the Studies on Energy Deposition for Application to the Problems of Supersonic Aerodynamics*, Preprint No. 10-2002, Khristianovich Inst. of Theoretical and Applied Mechanics, Novosibirsk, Russia, 2002.
[21] Fomin, V., Tretyakov, P., and Taran, J.-P., "Flow Control Using Various Plasma and Aerodynamic Approaches (Short Review)," *Aerospace Science and Technology*, Vol. 8, No. 5, July 2004, pp. 411–421.
doi:10.1016/j.ast.2004.01.005
[22] Bletzinger, P., Ganguly, B., Van Wie, D., and Garscadden, A., "Plasmas in High Speed Aerodynamics," *Journal of Physics D: Applied Physics*, Vol. 38, No. 4, Feb. 2005, pp. R33–R57.
doi:10.1088/0022-3727/38/4/R01
[23] Shang, J., "Recent Research in Magneto-Aerodynamics," *Progress in Aerospace Sciences*, Vol. 37, No. 1, Jan. 2001, pp. 1–20.
doi:10.1016/S0376-0421(00)00015-4
[24] Belokon, V., Rudenko, O., and Khokhlov, R., "Aerodynamic Effects of Supersonic Flow Past a Laser Beam," *Akusticheski Zhurnal*, Vol. 23, No. 4, July–Aug. 1977, pp. 632–634.
[25] Krasnobaev, K., and Syunyaev, R., "Calculation of Flow of Stellar Wind Past an X-Ray Source," *Mekhanika Zhidkosti i Gaza*, Vol. 4, July–Aug. 1983, pp. 106–111.
[26] Krasnobaev, K., "Supersonic Flow Past Sources of Radiation," *Mekhanika Zhidkosti i Gaza*, Vol. 4, July–Aug. 1984, pp. 133–136.
[27] Whitham, G., *Linear and Nonlinear Waves*, Wiley–Interscience, New York, 1974.
[28] Terent'eva, L., "Supersonic Flow Over Energy-Releasing Sources," *Mekhanika Zhidkosti i Gaza*, Vol. 5, Sept.–Oct. 1992, pp. 179–182.
[29] Vlasov, V., Grudnitskii, B., and Rygalin, V., "Gas Dynamics with Local Energy Release in Subsonic and Supersonic Flow," *Mekhanika Zhidkosti i Gaza*, No. 2, March–April 1995, pp. 142–148.
[30] Georgievskii, P., and Levin, V., "Supersonic Flow Over a Body with Heat Supply Ahead of It," *Proceedings of the Steklov Inst. of Mathematics*, Steklov Inst. of Mathematics, American Mathematical Society, Providence, RI, 1991, pp. 229–234.
[31] Knight, D., "Inviscid Compressible Flow," *The Handbook of Fluid Dynamics*, edited by R. Johnson, CRC Press, Boca Raton, FL, 1998.
[32] Georgievskii, P., and Levin, V., "Unsteady Effects for a Supersonic Flow Past a Pulsing Energy Source of High Power," *Proceedings of the 9th International Conference on Methods in Aerophysical Research*, Inst. of Theoretical and Applied Mechanics, Russian Academy of Sciences, Siberian Division, Novosibirsk, Russia, 1998, pp. 58–64.
[33] Charters, A., and Thomas, R., "The Aerodynamic Performance of Small Spheres from Subsonic to High Supersonic Velocities," *Journal of the Aeronautical Sciences*, Vol. 12, Oct. 1945, p. 468.
[34] Kolesnichenko, Y., Brovkin, V., Azarova, O., Grudnitsky, V., Lashkov, V., and Mashek, I., "Microwave Energy Release Regimes for Drag Reduction in Supersonic Flows," AIAA Paper 2002-0353, 2002.
[35] Kremeyer, K., Sebastian, K., and Shu, C.-W., "Lines of Pulsed Energy: Shock Mitigation and Drag Reduction," AIAA Paper 2004-1131, 2004.
[36] Plooster, M., "Shock Waves from Line Sources. Numerical Solutions and Experimental Measurements," *Physics of Fluids*, Vol. 13, No. 11, Nov. 1970, pp. 2665–2675.
doi:10.1063/1.1692848
[37] Artem'ev, V., Bergelson, V., Nemchinov, I., Orlova, T., Smirnov, V., and Khazins, V., "Modification of Regime of Flow over an Obstacle with a Thin Low-Pressure Channel Upstream," *Mekhanika Zhidkosti i Gaza*, Vol. 24, No. 1, 1989, p. 146.
[38] Borzov, V., Rybka, I., and Yur'ev, A., "Effect of Local Energy Supply in a Hypersonic Flow on the Drag of Bodies with Various Bluntness," *Inzhenerno-Fizicheski Zhurnal*, Vol. 67, Nos. 5–6, 1994, p. 355.
[39] Georgievskii, P., and Levin, V., "Supersonic Flow Past Bodies in the Presence of External Heat Supply Sources," *Letters to the Russian Journal of Applied Physics*, Vol. 14, 1988, p. 684.
[40] Georgievskii, P., and Levin, V., "Modification of Regime of the Flow over a Sphere by Means of Local Energy Supply Upstream," *Proceedings of the 8th International Conference on Methods in Aerophysical Research*, Inst. of Theoretical and Applied Mechanics, Russian Academy of Sciences, Siberian Division, Novosibirsk, Russia, 1996, pp. 67–73.
[41] Levin, V., and Terent'eva, L., "Supersonic Flow over a Cone with Heat Release in the Neighborhood of the Apex," *Mekhanika Zhidkosti i Gaza*, Vol. 2, March–April 1993, pp. 110–114.
[42] Toro, P., Myrabo, L., and Nagamatsu, H., "Pressure Investigation of the Hypersonic Directed-Energy Air Spike Inlet at Mach Number 10 up to 70 kW," AIAA Paper 98-0991, 1998.
[43] Myrabo, L., and Raizer, Y., "Laser-Induced Air Spike for Advanced Transatmospheric Vehicles," AIAA Paper 94-2451, 1994.
[44] Bracken, R., Myrabo, L., Nagamatsu, H., Meloney, E., and Shneider, M., "Experimental Investigation of an Electric Arc Air Spike in Mach 10 Flow with Preliminary Drag Measurements," AIAA Paper 2001-2734, 2001.
[45] Bracken, R., Myrabo, L., Nagamatsu, H., Meloney, E., and Shneider, M., "Experimental Investigation of an Electric Arc Air Spike with and Without Blunt Body in Hypersonic Flow," AIAA Paper 2001-0796, 2001.
[46] Levin, V., and Terent'eva, V., "Effect of a Local Energy Supply Region on 3-D Flow Around a Cone," *Mekhanika Zhidkosti i Gaza*, Vol. 3, No. 3, May–June 1999, pp. 106–113.
[47] Riggins, D., Nelson, H., and Johnson, E., "Blunt-Body Wave Drag Reduction Using Focused Energy Deposition," *AIAA Journal*, Vol. 37, No. 4, April 1999, pp. 460–467.
[48] Riggins, D., and Nelson, H., "Hypersonic Flow Control Using Upstream Focused Energy Deposition," *AIAA Journal*, Vol. 38, No. 4, April 2000, pp. 723–725.
[49] Shang, J., Hayes, J., and Menart, J., "Hypersonic Flow over a Blunt Body with Plasma Injection," AIAA Paper 2001-0344, 2001.
[50] Girgis, I., Schneider, M., Macheret, S., Brown, G., and Miles, R., "Creation of Steering Moments in Supersonic Flow by Off-Axis Plasma Heat Addition," AIAA Paper 2002-0129, 2002.
[51] Georgievskii, P., and Levin, V., "Control of the Flow Past Bodies Using Localized Energy Addition to the Supersonic Flow," *Fluid Dynamics*, Vol. 38, No. 5, 2003, pp. 794–805.
doi:10.1023/B:FLUI.0000007841.91654.10
[52] Georgievskii, P., and Levin, V., "Unsteady Interaction of a Sphere with Atmospheric Temperature Inhomogeneity at Supersonic Speed," *Mekhanika Zhidkosti i Gaza*, Vol. 4, No. 4, May–June 1993, pp. 174–183.
[53] Aleksandrov, A., Vidyakin, N., and Lakutin, V., "On a Possible Mechanism of Interaction of a Shock Wave with the Decaying Plasma of a Laser Spark in Air," *Zhurnal Tekhnicheskoi Fiziki*, Vol. 56, 1986, p. 771.
[54] Georgievskii, P., and Levin, V., "Bow Shock Wave Structures Control by Pulse-Periodic Energy Input," AIAA Paper 2004-1019, 2004.
[55] Tretyakov, P., Garanin, A., Kraynev, V., Tupikin, A., and Yakovlev, V., "Investigation of Local Laser Energy Release Influence on Supersonic Flow by Methods of Aerophysical Experiments," *Proceedings of the 8th International Conference on Methods in Aerophysical Research*, Inst. of Theoretical and Applied Mechanics, Russian Academy of Sciences, Siberian Division, Novosibirsk, Russia, 1996, pp. 200–204.
[56] Tretyakov, P., Kraynev, V., Yakovlev, V., Grachev, G., Ivanchenko, A., Ponomarenko, A., and Tischenko, V., "A Powerful Optical Pulsating Discharge as the Source of Energy Release in Supersonic Flow," *Proceedings of the 7th International Conference on Methods in Aerophysical Research*, Inst. of Theoretical and Applied Mechanics, Russian Academy of Sciences, Siberian Division, Novosibirsk, Russia, 1994, pp. 224–228.
[57] Levin, V., Afonina, N., and Gromov, V., "Navier-Stokes Analysis of Supersonic Flow with Local Energy Deposition," AIAA Paper 99-4967, 1999.
[58] Adelgren, R., Elliott, G., Knight, D., Zheltovodov, A., and Beutner, T., "Energy Deposition in Supersonic Flows," AIAA Paper 2001-0885, 2001.
[59] Adelgren, R., Elliott, G., Knight, D., Zheltovodov, A., and Buetner, T., "Localized Flow Control in Supersonic Flows by Pulsed Laser Energy Deposition," *The Third Workshop on Magneto- and Plasma Aerodynamics for Aerospace Applications*, Inst. for High Temperatures, Moscow, April 2001.
[60] Adelgren, R., "Localized Flow Control with Energy Deposition," Ph.D. Thesis, Dept. of Mechanical and Aerospace Engineering, Rutgers Univ., Sept. 2002.
[61] Exton, R., Balla, R., Shirinzadeh, B., Brauckmann, G., Hering, G., Kelliher, W., Fugitt, J., Lazard, C., and Khodataev, K., "On-Board Projection of a Microwave Plasma Upstream of a Mach 6 Bow Shock,"

Physics of Plasmas, Vol. 8, No. 11, Nov. 2001, pp. 5013–5017. doi:10.1063/1.1407819

[62] Kolesnichenko, Y., Brovkin, V., Leonov, S., Krylov, A., Lashkov, V., Mashek, I., Gorynya, A., and Ryvkin, M., "Investigation of AD-Body Interaction with Microwave Discharge in Supersonic Flows," AIAA Paper 2001-0345, 2001.

[63] Kolesnichenko, Y., Brovkin, V., Leonov, S., Krylov, A., Lashkov, V., Mashek, I., Gorynya, A., and Ryvkin, M., "Influence of Differently Organized Microwave Discharge on AD-Body Characteristics in Supersonic Flow," AIAA Paper 2001-3060, 2001.

[64] Kolesnichenko, Y., Brovkin, V., Khmara, D., Lashkov, V., Mashek, I., and Ryvkin, M., "Microwave Discharge Parameters in Supersonic Flow," AIAA Paper 2002-0356, 2002.

[65] Kolesnichenko, Y., Brovkin, V., Azarova, O., Grudnitsky, V., Lashkov, V., and Mashek, I., "MW Energy Deposition for Aerodynamic Application," AIAA Paper 2003-0361, 2003.

[66] Kolesnichenko, Y., Brovkin, V., Khmara, D., Lashkov, V., Mashek, I., and Ryvkin, M., "Fine Structure of MW Discharge: Evolution Scenario," AIAA Paper 2003-0362, 2003.

[67] Kolesnichenko, Y., Azarova, O., Brovkin, D., Khmara, D., Lashkov, V., Mashek, I., and Ryvkin, M., "Basics in Beamed MW Energy Deposition for Flow/Flight Control," AIAA Paper 2004-0669, 2004.

[68] Azarova, O., Grudnitsky, V., and Kolesnichenko, Y., "Some Gas Dynamic Aspects of Flow Control by MW Energy Deposition," *The Fifteenth International Conference on MHD Energy Conversion and Sixth Workshop on Magneto-Plasma-Aerodynamics in Aerospace Applications*, Inst. for High Temperatures, Russian Academy of Sciences, Moscow, May 2005, pp. 152–163.

[69] Leonov, S., Bityurin, V., Savischenko, N., Yuriev, A., and Gromov, V., "Influence of Surface Electrical Discharge on Friction of Plate in Subsonic and Transonic Airflow," AIAA Paper 2001-0640, 2001.

[70] Leonov, S., Bityurin, V., Savelkin, K., and Yarantsev, D., "Effect of Electrical Discharge on Separation Processes and Shocks Position in Supersonic Airflow," AIAA Paper 2002-0355, 2002.

[71] Zaidi, S., Shneider, M., Mansfield, D., Ionikh, Y., and Miles, R., "Influence of Upstream Pulsed Energy Deposition on Shock Wave Structure in Supersonic Flow," AIAA Paper 2002-2703, 2002.

[72] Kandala, R., and Candler, G., "Numerical Studies of Laser-Induced Energy Deposition for Supersonic Flow Control," *AIAA Journal*, Vol. 42, No. 11, Nov. 2004, pp. 2266–2275. doi:10.2514/1.6817

[73] Knight, D., Kolesnichenko, Y., Brovkin, V., and Khmara, D., "High Speed Flow Control Using Microwave Energy Deposition," AIAA Paper 2008-1354, 2008.

[74] Suchomel, C., and Van Wie, D., "Energy Based Performance Parameters for Hypersonic Flight Vehicles," AIAA Paper 2005-3277, 2005.

[75] Suchomel, C., Van Wie, D., and Brooks, G., "Energy Based Plasma Performance Specifications for Flight Vehicles," AIAA Paper 2006-3568, 2006.

[76] Suchomel, C., Van Wie, D., and Tejtel, D., "Assessment of Energetic Flow Control Techniques Using an Energy-Based Methodology," AIAA Paper 2007-7819, 2007.

[77] Yuriev, A., Korzh, S., Pirogov, S., Savischenko, N., Leonov, S., and Ryizhov, E., "Transonic Streamlining of Profile at Energy Addition in Supersonic Flow," *Third Workshop on Magneto-Plasma Aerodynamics for Aerospace Applications*, Inst. for High Temperatures, Moscow, April 2001, pp. 201–207.

S. Macheret
Associate Editor